NBSIR 75-822

STUDY OF ERRORS IN ABSOLUTE FLUX DENSITY MEASUREMENTS OF CASSIOPEIA A

Motohisa Kanda

Electromagnetics Division
Institute for Basic Standards
National Bureau of Standards
Boulder, Colorado 80302

October 1975

Prepared for:
Advanced Concepts Office
United States Army Communications Command
Fort Huachuca, Arizona 85613

NBSIR 75-822

STUDY OF ERRORS IN ABSOLUTE FLUX DENSITY MEASUREMENTS OF CASSIOPEIA A

Motohisa Kanda

Electromagnetics Division
Institute for Basic Standards
National Bureau of Standards
Boulder, Colorado 80302

October 1975

Prepared for:
Advanced Concepts Office
United States Army Communications Command
Fort Huachuca, Arizona 85613

U.S. DEPARTMENT OF COMMERCE, Rogers C. B. Morton, Secretary
James A. Baker, III, Under Secretary
Dr. Betsy Ancker-Johnson, Assistant Secretary for Science and Technology

NATIONAL BUREAU OF STANDARDS, Ernest Ambler, Acting Director

CONTENTS

LIST OF FIGURES

STUDY OF ERRORS IN ABSOLUTE FLUX DENSITY MEASUREMENTS OF CASSIOPEIA A

Motohisa Kanda

An error analysis for absolute flux density measurements of Cassiopeia A is discussed. The lower-bound quadrature-accumulation error for state-of-the-art measurements of the absolute flux density of Cas A around 7 GHz is estimated to be 1.71% for 3σ limits. The corresponding practicable error for the careful but not state-of-the-art measurement is estimated to be 4.46% for 3σ limits.

Key words: Accuracy; antenna; calibration; Cassiopeia A; error analysis; flux density, G/T (system gain/system noise temperature); ground station; radio star.

I. Introduction

Strong cosmic "point" radio stars, such as Cassiopeia A, (Cas A), Cygnus A (Cyg A), Taurus A (Tau A), etc., provide accurately positioned broadband noise standards for G/T (system gain/system noise temperature) measurements on large ground stations. Especially, the small angular size (approximately 4 arc-minutes) and the strong flux render Cas A useful for the measurements of G (system gain) and G/T. The success of the measurement depends to a large extent on good knowledge and proper evaluation of the properties of Cas A used as a standard noise source.

In order to measure the absolute values of G and G/T for a large ground station, the absolute flux density of the radio star is required. Considerable effort has been devoted to establish the absolute flux density of Cas A [Allen et al. 1967; Baars 1973; Baars et al. 1972; 1965; Broten et al. 1960; Findlay 1972; 1966; Findlay et al. 1965; Kellerman et al. 1969; Medd 1972; Medd et al. 1965; Pawsey 1955; Penzias et al. 1965]. However, comparisons among various sets of observations are often complicated by a lack of agreement on the scales of the absolute flux density, and, moreover, all the observations have not been of comparable accuracy. Sometimes the problems are compounded by the fact that the accuracy and the precision of the measurements are confused. In addition, a random error estimate which specifies the precision of a measurement is not often clearly identified as to whether it is for 1σ, 3σ or something else.

The purpose of this paper is to discuss the potential accuracy of the absolute flux density measurements of Cas A around 7 GHz. By use of a precise brightness temperature contour map of Cas A, all the correction factors for the absolute flux density measurements are analyzed in detail. This paper will first discuss the theoretical development for the absolute flux density measurements and then the corresponding detailed error analysis.

II. Theoretical Developments

In general, the absolute measurements of the flux density of Cas A consist of the following six steps (e.g., Allen et al. 1967; Broten et al. 1960; Findlay et al. 1964; Medd 1972): 1) measuring the system output, $W_{d,1}$, when the antenna is pointing at Cas A; 2) measuring the system output, $W_{d,2}$, when the antenna is pointing away from Cas A; 3) taking the difference, $\Delta W_{\text{Cas A}}$, between $W_{d,1}$ and $W_{d,2}$; 4) measuring the system outputs $W_{\text{Cal},3}$ and $W_{\text{Cal},4}$ when the input of the radiometer is connected in succession to two thermal noise standards with different noise temperatures; 5) taking the difference, ΔW_{Cal}, between $W_{\text{Cal},3}$ and $W_{\text{Cal},4}$; 6) finally taking the ratio, Y, of $\Delta W_{\text{Cas A}}$ to ΔW_{Cal}. The measurement scheme is shown in figure 1. Each measurement step is discussed below in detail.

During the transit of Cas A, the available spectral power at the antenna output port, $W_{a,1}(f)$ in watts per hertz, is given by the antenna convolution integral;

$$W_{a,1}(f,\Omega_o) = kT_1(f) + M_p(f)A_e(f) \int \alpha(f,\Omega)B(f,\Omega)P_n(f,\Omega-\Omega_o)\, d\Omega, \qquad (1)$$

where

$$M_p(f) = \frac{1}{2} + \frac{d(f)}{2}[\cos 2\varepsilon_w(f) \cos 2\varepsilon_a(f) \cos 2[\tau_w(f)-\tau_a(f)] + \sin 2\varepsilon_w(f) \sin 2\varepsilon_a(f)]. \qquad (2)$$

The symbols have the following meanings: k is Boltzmann's constant ($= 1.38\text{x}10^{-23}$ J K^{-1}); $T_1(f)$ is the system (minus receiver) noise temperature with the antenna pointing at Cas A in kelvins; $M_p(f)$ is the polarization mismatch factor; $A_e(f)$ is the effective area of an antenna in square meters, d(f) is the degree of polarization of the source, defined as the ratio of the completely polarized power to the total power; $\varepsilon(f)$ and $\tau(f)$ are referred to, respectively, as the polarization angle and the tilt angle, and are specified in figure 2; $\alpha(f,\Omega)$ is the atmospheric transmission coefficient; $B(f,\Omega)$ is the brightness of Cas A in Wm^{-2} Hz^{-1} rad^{-2}; $P_n(f,\Omega-\Omega_o)$ is the normalized antenna power pattern in which the difference "$\Omega-\Omega_o$" reflects the fact that the antenna may not be pointing towards the center, Ω_o, of Cas A. The subscripts w and a on ε and τ denote factors associated with the wave and receiving antenna, respectively. By introducing the delivered power-to-available power system gain, g(f), i.e.,

$$g(f) = \frac{\text{Delivered power at the system output port}}{\text{Available power at the antenna output port}} \qquad (3)$$

the delivered power from the output port of the receiver when the antenna is pointing at Cas A is

$$W_{d,1} = k \int [T_1(f) + T_{e,1}(f)]g_1(f)\, df + \int df\, M_p(f)A_e(f)g_1(f) \int d\Omega\, \alpha(f,\Omega)B(f,\Omega)P_n(f,\Omega-\Omega_o)\, d\Omega \quad (4)$$

where $T_e(f)$ is the effective input noise temperature of the radiometer.

When the antenna is pointing away from Cas A, the delivered power from the output is given by

$$W_{d2} = k \int [T_2(f) + T_{e,2}(f)]\, g_2(f)\, df \quad (5)$$

where $T_2(f)$ is the system (minus receiver) noise temperature with the antenna pointing away from Cas A.

The delivered power contributed solely by Cas A is then determined by the difference between $W_{d,1}$ and $W_{d,2}$, i.e.,

$$\begin{aligned} \Delta W_{\text{Cas A}} &\equiv W_{d,1} - W_{d,2} \\ &= k \int [T_1(f)g_1(f) - T_2(f)g_2(f)]\, df \\ &+ k \int [T_{e,1}(f)g_1(f) - T_{e,2}(f)g_2(f)]\, df \\ &+ \int df\, M_p(f)A_e(f)g_1(f) \\ &\times \int d\Omega\, \alpha(f,\Omega)B(f,\Omega)P_n(f,\Omega-\Omega_o) \end{aligned} \quad (6)$$

The calibration of the radiometer is accomplished, in principle, by use of two standard noise sources. For example, the scheme shown in figure 1 will calibrate the radiometer. When the input of the radiometer is disconnected from the antenna and is connected in succession to two thermal noise standards with different noise temperatures, the delivered powers from the output of the radiometer are

$$W_{cal,3} = k \int [T_{cal,3}(f) + T_{e,3}(f)]g_3(f)\, df, \quad (7)$$

and

$$W_{cal,4} = k \int [T_{cal,4}(f) + T_{e,4}(f)]g_4(f)\, df, \quad (8)$$

where T_{cal} is the available noise temperature of the thermal noise standard. The difference between $W_{cal,3}$ and $W_{cal,4}$ is,

$$\begin{aligned} \Delta W_{cal} &\equiv W_{cal,3} - W_{cal,4} \\ &= k \int [T_{cal,3}(f)g_3(f) - T_{cal,4}(f)g_4(f)]\, df \\ &+ k \int [T_{e,3}(f)g_3(f) - T_{e,4}(f)g_4(f)]\, df. \end{aligned} \quad (9)$$

By taking the ratio of $\Delta W_{Cas\ A}$ to ΔW_{cal},

$$Y \equiv \frac{\Delta W_{Cas\ A}}{\Delta W_{cal}}$$

$$= \frac{k \int (T_1 g_1 - T_2 g_2) df + k \int (T_{e,1} g_1 - T_{e,2} g_2)\ df}{k \int [T_{cal,3}(f) g_3(f) - T_{cal,4}(f) g_4(f)]\ df} \qquad (10)$$

$$+ \frac{\int df\ M_p(f) A_e(f) g_1(f) \int d\Omega\ \alpha(f,\Omega) B(f,\Omega) P_n(f,\Omega-\Omega_o)}{+ k \int [T_{e,3}(f) g_3(f) - T_{e,4}(f) g_4(f)]\ df}$$

Using eq. (10), the total source flux density, S, of Cas A is given by

$$S = \iint B(\Omega)\ d\Omega = \frac{2k}{A_e} \frac{T_{cal,3} - T_{cal,4}}{k_1 \ldots k_7} Y. \qquad (11)$$

The k_1 through k_7 are correction factors which are listed below:

k_1 = Atmospheric transmission factor,
k_2 = Star shape factor,
k_3 = Bandwidth factor,
k_4 = Differential sky brightness temperature factor,
k_5 = Antenna pointing factor,
k_6 = Polarization factor,
k_7 = System response factor.

Using the precise brightness temperature contour map of Cas A, all the correction factors and their accuracies are next analyzed in detail.

III. Correction Factors and Their Accuracies

The knowledge of the power gain and the corresponding effective area of the standard gain antenna is basic to the problem. The measurement of the power gain of the large standard antenna is one of the difficult tasks in radio engineering. Accuracy considerations in the measurement of the antenna power gain are discussed by the author (Kanda 1975; Wait et al. 1974). Uncertainties in the value of standard noise temperatures and in the ratio measurement, Y, are also important sources of error. These uncertainties are summarized in § IV. In this section, all the correction factors and their errors are analyzed by use of the precise brightness temperature contour map of Cas A published by Rosenberg (1970b).

a. Star Shape Factor--k_2

The star shape factor k_2 is given by

$$k_2 = \frac{\int B(\Omega)\ P_n(\Omega)\ d\Omega}{\int B(\Omega)\ d\Omega} \tag{12}$$

where $B(\Omega)$ is the brightness of Cas A, and $P_n(\Omega)$ is the normalized antenna power pattern. Cas A is usually assumed to be a uniform disk with the resulting star shape correction factor approximated by (Baars et al. 1965)

$$k_2 \cong \frac{1-e^{-x^2}}{x^2} \tag{13}$$

where

$$x = \frac{D}{1.2012\ \theta_{hp}} \tag{14}$$

and D is the angular diameter of Cas A and θ_{hp} is the half-power-beamwidth of the antenna. However, because Cas A is not a uniformly radiating disk, but rather an anomalous source of radio waves where a large percentage of the power is radiated from a circularly shaped ridge, a means must be devised for estimating the magnitude of error caused by this assumption.

Figure 3 shows the brightness temperature contour map of Cas A measured at epoch AD 1950.0 (Rosenberg 1970b), where the thick dashed curve represents the zero contour relative to a cold area of the sky well separated from the source, and where the contour interval is 200 kelvins. The brightness temperature is plotted in declination versus right ascension, and the highly structured nature of Cas A is clearly evident. It is clear that the source is well localized with a slight bulge towards the east (upper center). The high-resolution maps of Cas A show that all of the parameters of Cas A, flux density, spectral index, degree of polarization and position angle, and secular decay rate, which are considered to be constants in the broad antenna beamwidth picture, do in fact vary across the face of the source in a highly irregular manner (Rosenberg 1970a, 1970b).

The brightness temperature contour map of Cas A shown in figure 3 is reduced to numerical values by a superimposed grid with a value assigned for each intersection of a horizontal and vertical line. This numerical representation is fed into a computer which reconstructs a comparable brightness temperature contour map, and the result is shown in figure 4. From this numerical representation, the computer plots out the relative brightness temperature of Cas A in a three-dimensional representation which is shown in figure 5.

Using the computer-stored representation of Cas A it is possible to convolute the star shape with the antenna power pattern to determine the magnitude of the error caused by assuming a uniform disk for Cas A. In the convolution integral, it is assumed that the normalized antenna power pattern can be very closely approximated by the sinc x function. Knowing that the function $\text{sinc}^2 x \cong 0.5$ when $x \cong 1.392$ radian, the normalized antenna power pattern is given by

$$P(\theta,\phi) = \text{sinc}^2\left(\frac{2.784\theta}{\theta_{hp}}\right) \text{sinc}^2\left(\frac{2.784\theta}{\phi_{hp}}\right), \qquad (15)$$

where θ_{hp} and ϕ_{hp} represent the half-power-beamwidth of the antenna.

Figure 6 shows the three-dimensional representation of numerical convolution integral of Cas A with an antenna whose half-power-beamwidth is 2 minutes. With this antenna, Cas A is still a discrete source with some structure with maximum coupling observed toward the east. However, with an antenna of 4 minute half-power-beamwidth, the shape of the result for the numerical convolution integral is very similar to that of the normalized antenna power pattern itself as shown in figure 7 in three-dimensional presentation, and Cas A can now be treated as a discrete source without structure. For further reference, the three-dimensional representation of the numerical convolution integral with an antenna of 6 minute half-power-beamwidth is shown in figure 8.

To determine the most appropriate equivalent disk size for Cas A, the star shape factor using the actual brightness temperature contour map shown in figure 4 and using a uniformly radiating 4.3 minute disk in eq. (13) are shown in figure 9 as functions of antenna-half-power beamwidth. This 4.3 minute uniformly radiating disk has been commonly used by radio astronomers (e.g., Baars et al. 1965). The discrepancies between the star shape correction factor using a precise brightness temperature contour map of Cas A and that using a uniformly radiating disk distribution of various disk sizes are shown in figure 10. It is found from this figure that, contrary to the 4.3 minute disk which radio astronomers have been commonly using, the choice of 4.6 minutes for the disk size gives less error in the star shape factor. For an antenna of half-power-beamwidth larger than 4.6 minutes, the error by using a 4.6 minute disk distribution is at most 0.2%. It is also found from figure 10 that the star shape correction for an antenna with a half-power beamwidth less than 4.6 minutes is very large (i.e., k_2 is much less than one), and, therefore, the error associated with the correction factor is expected to be large.

From the explanation above, it is very natural to assume that the most appropriate estimate for the size of Cas A is about 4.6 minute. This agrees remarkably well with the mean radial profile shown in figure 11 (Rosenberg 1970b). This mean profile of the map was obtained by averaging the emission from annuli 5 arc seconds wide drawn from the center of the shell, and the

edge of the shell turns out to be approximately 140 seconds of arc from the center, which corresponds to a 4.6 minute diameter for Cas A.

b. Antenna Pointing Factor--k_5

When the antenna is pointing slightly off the center of the radio star by an amount Ω_o, the system output will then be reduced by an amount

$$k_5 = \frac{\int B(\Omega)\ P_n(\Omega-\Omega_o)\ d\Omega}{\int B(\Omega)\ P_n(\Omega)\ d\Omega}. \qquad (16)$$

If the antenna pointing is highly accurate, the antenna can be pointed at the center of the source (defined as the point of maximum antenna temperature) and k_5 is near unity. For example, convoluting the brightness temperature contour map of Cas A shown in figure 4 with a gaussian antenna power pattern places the center of Cas A at $23^h21^m20^s$ RA (α) and 58°32'30" DEC (δ). These values are only slightly different from the optical center of the Cas A nebulosities $23^h21^m11^s.4$ and 58°32'18".9 (Rosenberg 1970b).

The antenna pointing factor for the measurement of the flux density of Cas A is calculated by use of eq. (16) with the brightness temperature contour map shown in figure 5, and is shown in figure 12. It is found from this figure that a typical antenna pointing accuracy of 5% in terms of half-power beamwidth gives rise to 0.7% error in the measurement of the flux density.

When the antenna pointing accuracy is not high, k_5 can differ appreciably from unity and is therefore difficult to calculate accurately. In this case star drift measurements can be used to circumvent the difficulty. Using a drift measurement technique, the antenna pointing factor, k_5, is shown in figure 13 as a function of a number of drift cuts across Cas A. It is found from this figure that, for an antenna with half-power beamwidth of 6 minutes or greater, five drift cuts across Cas A are minimum and optimum, and give rise to a reasonable accuracy. More than five drift cuts will not provide any significant advantages in determining the antenna pointing factor accurately. It is found from figure 13 that by taking five drift measurements approximately one minute apart and fitting their peaks to a Gaussian curve, it is possible to estimate the antenna pointing factor, k_5, to within 0.5% for an antenna with a half-power of beamwidths 6 minutes or greater.

It should be pointed out that this drift measurement technique is also a very useful technique to determine the half-power beamwidth of an antenna. Figure 14 shows how the width of the Gaussian fit for a drift curve changes with different (in declination) cuts across Cas A. This figure indicates that, for an antenna with a half-power-beamwidth 4 minutes or less, the width of the Gaussian fit for a drift curve does change with the location of the drift cut across Cas A. However, it is found from figure 15 that, for an antenna with

a half-power beamwidth of 6 minutes or greater, the width of the Gaussian fit is constant regardless of where the location of the drift cut across Cas A is and how large the half-power beamwidth of an antenna is, provided that the main beam of the antenna power pattern is approximated by the Gaussian function.

c. Atmospheric Transmission Factor--k_1

As electromagnetic waves from Cas A pass through the atmosphere to the antenna, they are attenuated. The atmospheric transmission factor, k_1, accounts for the atmospheric reduction in the star flux density between the upper reaches of the atmosphere and the antenna aperture at microwave frequencies, and is given by (Daywitt 1975)

$$k_1 = k_d k_g k_r \tag{17}$$

where k_d, k_g, k_r are the transmission factors corresponding to atmospheric diffusion, atmospheric gas absorption, and atmospheric refraction, respectively. To obtain the best accuracy it is assumed that measurements are performed only at high elevation angles on clear days.

The details of the calculation and error analysis are discussed by Daywitt (1975). The atmospheric transmission factor error above 5 degrees at 7 GHz for an antenna with a half-power beamwidth of 10 minutes is shown in figure 16.

d. Differential Sky Brightness Temperature Factor--k_4

Since Cas A, Cyg A, and Tau A are all located close to the galactic plane, special care must be taken with the cosmic background effect, particularly at lower frequencies. In principle, the sky brightness temperature, T_1, when the antenna is pointing at Cas A and the sky brightness temperature, T_2, when the antenna is pointed off Cas A, are different. The difference between T_1 and T_2 leads to the differential sky brightness temperature factor and is given by

$$k_4 = 1 + \frac{T_1 - T_2}{\frac{A_e}{2k} \int B(\Omega)\, P_n(\Omega)\, d\Omega}. \tag{18}$$

It should be noted that in the drift measurements the noise temperature difference $T_1 - T_2$ is due solely to the changing cosmic background as Cas A passes through the antenna beam. To illustrate the magnitude of the difference between T_1 and T_2, a detailed radio emission contour map of the region around Cas A is shown in figure 17 (RaghavaRao et al. 1965). The contour intervals are designated by integers which are multiples of 0.87 kelvin above a uniform background of 3 kelvin black-body radiation. Since the brightness for the HII (ionized hydrogen) region is approximately flat above 1 GHz, T_1-T_2 can be estimated by 0.9 kelvin per square frequency in GHz.

Assuming that:

1) the flux density S(f) of Cas A can be expressed as (e.g., Wait et al. 1974)

$$S(f) = 3604 \times 10^{-26} f^{-0.875} \text{ Wm}^{-2} \text{ Hz}^{-1} \tag{19}$$

where f is a frequency in GHz, and

2) the approximate relationship among the power gain, G, the effective area, A_e, and the half-power-beamwidth, θ_{hp}, in minutes are given by

$$G = \frac{4\pi A_e}{\lambda^2} \cong \frac{9.578 \times 10^7}{\theta_{hp}^2}, \tag{20}$$

the differential sky brightness temperature factor, k_4, is then approximately given by

$$k_4 \cong 1 + \frac{1.52 \times 10^{-5} f^{0.88}}{1 - e^{-14.7/\theta_{hp}^2}} \tag{21}$$

where f is the frequency in GHz and θ_{hp} is the antenna half-power beamwidth in minutes. The differential sky brightness temperature factor, k_4, is shown in figure 18 as a function of half-power beamwidth of an antenna.

e. Polarization Factor--k_6

When the polarized component of the radiation from Cas A and the receiving antenna polarization are not matched, it is necessary to introduce the polarization factor, k_6, to account for the polarization mismatch. Assuming that the degree of polarization, the polarization angle and the tilt angle do not change appreciably with frequency within a small bandwidth and over the entire solid angle subtended at the antenna by Cas A, the polarization correction factor, k_6, is given approximately by

$$k_6 \cong 2M_p = 1 + d[\cos 2\varepsilon_w \cos 2\varepsilon_a \cos 2(\tau_w - \tau_a) + \sin 2\varepsilon_w \sin 2\varepsilon_a]. \tag{22}$$

The polarization correction factor for special combinations of antennas and waves are compared in table 1.

Table 1

Polarization Correction Factor

Wave Polarization	Antenna Polarization	Linear (ε_a=0)	Right Circular (ε_a=-45°)	Left Circular (ε_a=45°)
Linear	(ε_w=0)	$1+d\cos 2(\tau_w-\tau_a)$	1	1
Right Circular	(ε_w=-45°)	1	1+d	1-d
Left Circular	(ε_w=45°)	1	1-d	1+d

The literature suggests that above 1 GHz the linear polarization of Cas A is approximately 1% and that below 1 GHz the polarization falls to zero. Table 2 is representative of the values reported.

Table 2

Degree of Linear Polarization of Cas A

Frequency (GHz)	Polarization (%)	Reference
1	< 1	(Baars 1973)
3	< 1	(Baars 1973)
5	1.4 ± 0.5	(Rosenberg 1970b)
8.25	0.5 ± 0.2	(Allen et al. 1967)
10	1.5	(Baars 1973)
14.5	1.2 ± 0.5	(Boland et al. 1966)
15.25	1.9 ± 0.2	(Allen et al. 1967)
15.75	2.2 ± 0.3	(Allen et al. 1967)
19.4	1	(Mayer et al. 1968)

The degree of antenna polarization is commonly expressed in terms of axial ratio, A, rather than polarization angle, ε, and one can arrive at the well-known relation (Kraus et al. 1966)

$$A = \cot \varepsilon = \frac{E_\ell + E_r}{E_\ell - E_r} \tag{23}$$

where E_ℓ and E_r are, respectively, left and right circularly polarized field components. For a non-ideally circularly polarized antenna with partially linearly polarized waves from Cas A, the polarization correction factor, k_6, is then given by

$$k_6 \cong 1 + d \cos 2(\cot^{-1} A). \tag{24}$$

Assuming that the axial ratio, A, of the standard gain antenna is 1.1 and the linear polarization of Cas A above 1 GHz is 1%, the error in the polarization correction factor k_6 is no more than 0.1%.

f. Bandwidth Factor--k_3

The frequency variation of the various parameters that comprise the elements of eq. (10) across the system bandwidth lead to the bandwidth correction. Assuming that the passband of a receiving system has a square window and the power gain of the antenna is nominally 60 dB around 7 GHz which corresponds to an effective area of 145 m^2, the bandwidth correction factor is given approximately by

$$k_3 \cong 1 + (\Delta f/2f_o)^2, \tag{25}$$

when Δf is the bandwidth of a square pass band and f_o is its center frequency. In the case of a 50 MHz bandwidth at a center frequency of 7 GHz, the bandwidth correction factor, k_3, is very close to unity.

g. System Response Factor--k_7

Instabilities due to receiver gain and its effective input noise temperature are often significant sources of error in the measurement of the flux density of Cas A. In order to minimize the measurement errors, extremely good receiver stability is required. Instabilities due to receiver gain and its effective input noise temperature leads to the system response factor, k_7. By assuming that the pass band of the receiving system has a square window, and both the effective input noise temperature of the receiving system and the noise temperature of the standard noise sources are independent of frequency within a small bandwidth, the system response factor is then given approximately by

$$k_7 \cong 1 \pm \left|\frac{\Delta g}{g}\,\frac{\Delta T_e}{T_e}\right|\left(\frac{2kT_e}{A_e S} + \frac{T_e}{T_{cal,3}-T_{cal,4}}\right) \tag{26}$$

where $\Delta g/g$ is the fractional change in the system gain and $\Delta T_e/T_e$ is the fractional change in the effective input noise temperature of the receiving system. Assuming that $(\Delta g/g)\cdot(\Delta T_e/T_e) = 0.1\%$ (3σ), $S = 656 \times 10^{-26}$ Wm^{-2} Hz^{-1} at 7 GHz, $A_e = 145$ m^2 at 7 GHz, $T_e = 30$ K, $T_{cal,3} = 300$ K, $T_{cal,4} = 290$ K, k_7 is approximately equal to $1\pm(0.4\%)(3\sigma)$.

In addition to instability of gain and effective input noise temperature of the receiving system, the system response factor, k_7, should include a component due to resolution. The resolution component can be estimated by $(T_{Cas\ A} + T_{sys})/\sqrt{B\tau}$, where $T_{Cas\ A}$ is the temperature rise due to Cas A, T_{sys}

is the system noise temperature, B is the bandwidth, and τ is the time constant of the receiving system. Assuming that $T_{Cas\ A}$ = 36 K, T_{sys} = 150 K, B = 50 MHz, and τ = 1 sec., the uncertainty due to resolution is approximately 0.1%.

In the drift measurements the integrator of the radiometer distorts the drift curve. The results of the distortion are a shift in the position of the maximum with a decrease in its value and a broadening of the drift curve. The amount of distortion depends on the integration time constant and the time it takes the antenna to pass through Cas A. The detailed analysis on this subject is discussed by Kuz'min et al. (1966). When the time constant is on the order of one second and the half-power transit time is on the order of two minutes, the integration effect due to the time constant can be neglected.

IV. Error Analysis

An estimate of the limiting error for the calibration of the flux density of Cas A around 7 GHz is summarized in table 3. Since all the contributing sources of error are independent and, therefore, satisfy the condition for quadrature error addition, the total error indicated in table 3 is a quadrature-accumulation error.

Table 3

The Error in Measuring the Absolute Flux Density of Cas A Around 7 GHz

Sources of Error	Uncertainty in Value of Quantity		Error Contributing to Measuring Flux Density of Cas A	
	Lower Bound	Practicable	Lower Bound	Practicable
1. Antenna Power Gain	60 0.06 dB	60 0.18 dB	1.39%	4.23%
2. Temperature Calibration Standard	0.1K		0.03%	
3. Y Factor	0.002 dB		0.05%	
4. Atmospheric Transmission Factor k_1	0.99 0.005	0.99 0.01	0.51%	1.01%
5. Star Size Factor k_2	0.9314 0.0044		0.47%	
6. Bandwidth Factor k_3	1 0.0001		0.01%	
7. Differential Sky Brightness Temperature Factor k_4	1 0.0006		0.06%	
8. Antenna Pointing Factor k_5	1 0.005		0.5%	
9. Polarization Factor k_6	1 0.001	1 0.01	0.1%	0.5%
10. System Response Factor k_7	1 0.005(3)		0.5%	
Quadrature-Accumulation Error			1.71%	4.46%

In the analysis of the error estimate, the following assumptions are made:

1) The standard gain antenna with a power gain of nominally 60 dB around 7 GHz is calibrated to within a quadrature accumulation error of 0.06 dB for 3σ limits (Kanda 1975; Wait et al. 1974). This lower bound estimate is based on an ideal state-of-the-art measurement condition. The practicable error for the standard gain antenna measurement which is based on careful but not quite state-of-the-art conditions is estimated to be 0.18 dB for 3σ limits (Kanda 1975; Wait et al. 1974).

2) The measurement of power ratio Y in eqs. (10) and (11) utilizes an automated measuring system (Boyle et al. 1972) developed around the most accurate power measurement bridge known -- the NBS Type II self-balancing bridge (Larsen et al. 1970). This bridge measures the ratio of stable noise powers to an estimated error not greater than ± 0.002 dB (Wait et al. 1974).

3) The total uncertainty in the noise temperatures of standard noise sources (e.g., 290 K and 300 K) is no greater than 0.1 K, i.e., 0.03%.

With these assumptions, it seems possible to calibrate the flux density of Cas A around 7 GHz to within a quadrature-accumulation error of 1.71% for 3σ limits. This is a good estimate of the lower-bound of the uncertainty based on the state-of-the-art measurements. The corresponding practicable error for the careful but not state-of-the-art measurements is estimated to be 4.46% for 3σ limits.

V. Conclusion

It has been found that the absolute flux density of Cas A around 7 GHz can be measured to within a quadrature-accumulation error of 1.71% for 3σ limits from the assumption that the standard gain antenna of nominally 60 dB gain can be calibrated to within a quadrature accumulation error of 0.06 dB for 3σ limits. This procedure has established a lower-bound on the standard error for the state-of-the-art measurement of the absolute flux density of Cas A, in which a 3σ random error estimate has been included along with the various systematic errors. The practicable error for the standard gain antenna measurement which is based on careful but not quite state-of-the-art conditions is estimated to be 0.18 dB for 3σ limits. In this case, the practicable error for the measurements of the absolute flux density of Cas A around 7 GHz is estimated to be 4.46% for 3σ limits.

VI. Acknowledgment

The author wishes to thank B.K. Bender for her computer assistance, and W.D. Daywitt and D.F. Wait for many stimulating discussions in the preparation of this manuscript. Appreciation is also extended to C.K.S. Miller for his continuing support in this subject.

References

Allen, R.J. and Barrett, A.H. (1967) Astrophysical Journal, 149, 1-13.

Baars, J.W.M. (1973) IEEE Trans. Antennas & Propagation, AP-21, 461-474.

Baars, J.W.M. and Hartsuijker, A.P. (1972) Astronomy and Astrophysics, 17, 172-181.

Baars, J.W.M., Mezger, P.G., and Wendker, H. (1965) Astrophysical Journal, 142, 122-134.

Boland, J.W., Hollinger, J.P., Mayer, C.H. and McCullough T.P. (1966) Astrophysical Journal, 144, 437-439.

Boyle, D.R., Clague, F.R., Reeve, G.R., Wait, D.F. and Kanda, M. (1972) IEEE Trans. on Instrumentation and Measurement, IM-21, 543-549.

Broten, N.W. and Medd, W.J. (1960) Astrophysical Journal, 132, 279-285.

Daywitt, W.C. (1975) "Basic Error Equations for NBS G/T Measurements," NBSIR, to be published.

Findlay, J.W. (1966) Ann. Review Astronomy & Astrophysics, 4, 77-93.

Findlay, J.W. (1972) Astrophysical Journal, 174, 527-528.

Findlay, J.W., Huatum, H. and Waltman, W.B. (1965) Astrophysical Journal, 141, 873-884.

Kanda, M. (1975) IEEE Trans. Antennas & Propagation, AP-23, 407-411.

Kellerman, K.I., Pauling-Toth, I.I.K. and Williams, P.J.S. (1969) Astrophysical Journal, 157, 1-34.

Kraus, J.D. and Tiuri, M.E. (1966) Radio Astronomy (McGraw-Hill Book Company, New York) 108-130.

Kuz'min, A.D. and Salomonovich, A.E. (1966) Radioastronomical Methods of Antenna Measurements (Academic Press, New York) 89-92.

Larson, N.T. and Clague, F.R. (1970) Proc. 1970 ISA Annual Conf., 25, 712-770.

Mayer, C.H. and Hollinger, J.P. (1968) Astrophysical Journal, 151, 53-63.

Medd, W.J. (1972) Astrophysical Journal, 171, 41-50.

Medd, W.J. and Ramanov, K.V.V. (1965) Astrophysical Journal, 142, 383-386.

Pawsey, J.L. (1955) Astrophysical Journal, 121, 1-5.

Penzias, A.A. and Wilson, R.W. (1965) Astrophysical Journal, 142, 1149-1155.

RaghavaRao, R., Medd, W.J., Higgs, L.A. and Broten, N.W. (1965) Royal Astronomical Society Monthly Notices, 129, 159-168.

Rosenberg, I. (1970a) Royal Astronomical Society Monthly Notices, 147, 215-230.

Rosenberg, I. (1970b) Royal Astronomical Society Monthly Notices, 151, 109-122.

Wait, D.F., Daywitt, W.C., Kanda, M. and Miller C.K.S. (1974) NBSIR 74-382.

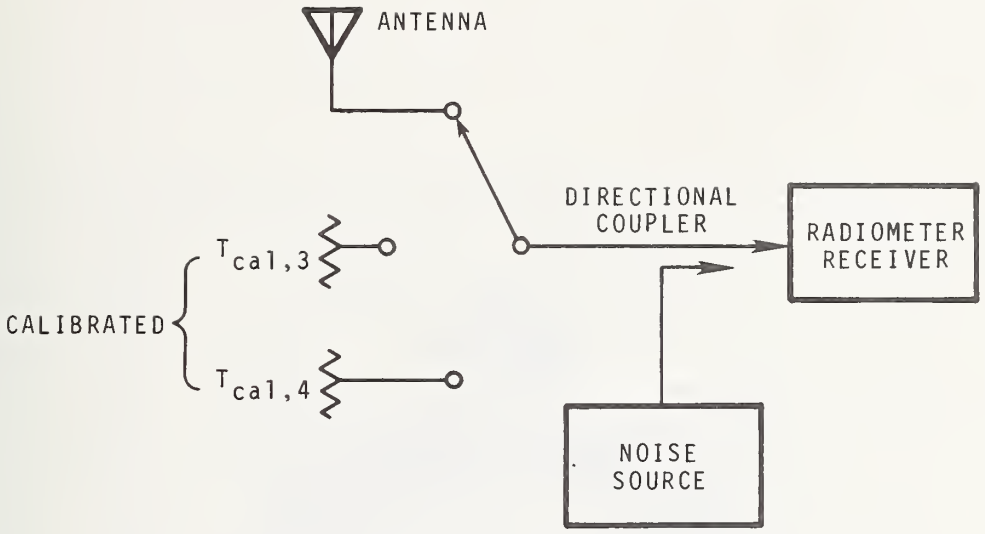

Figure 1. Block diagram of the measurement system

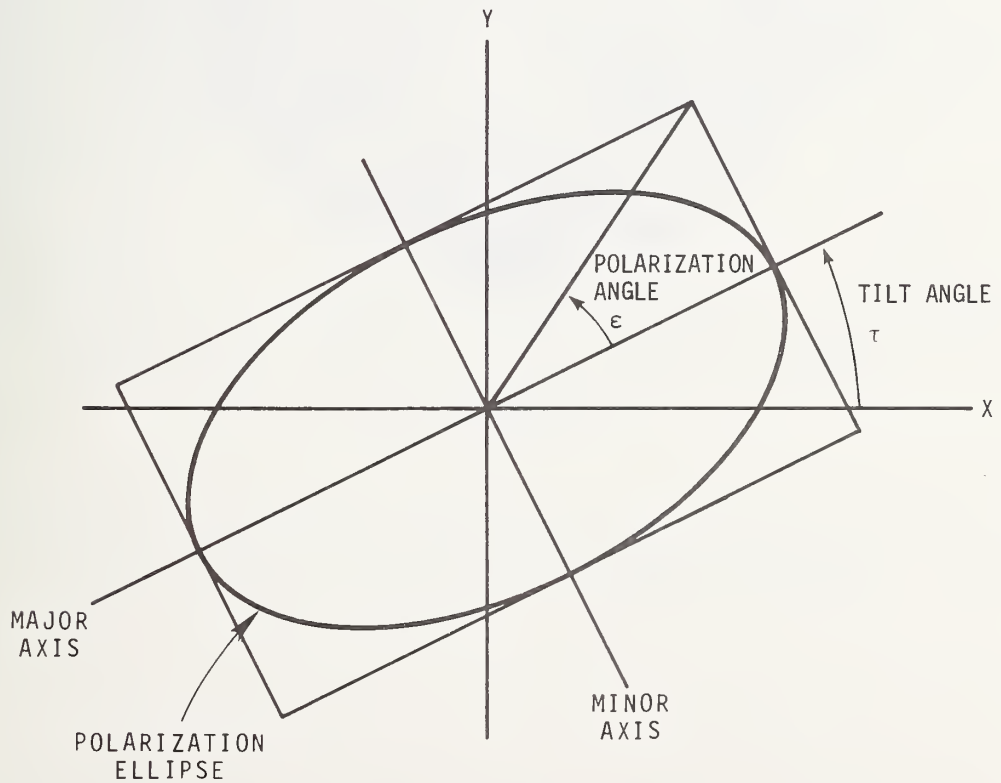

Figure 2. Relation of the polarization angle ε and tilt angle τ to the polarization ellipse

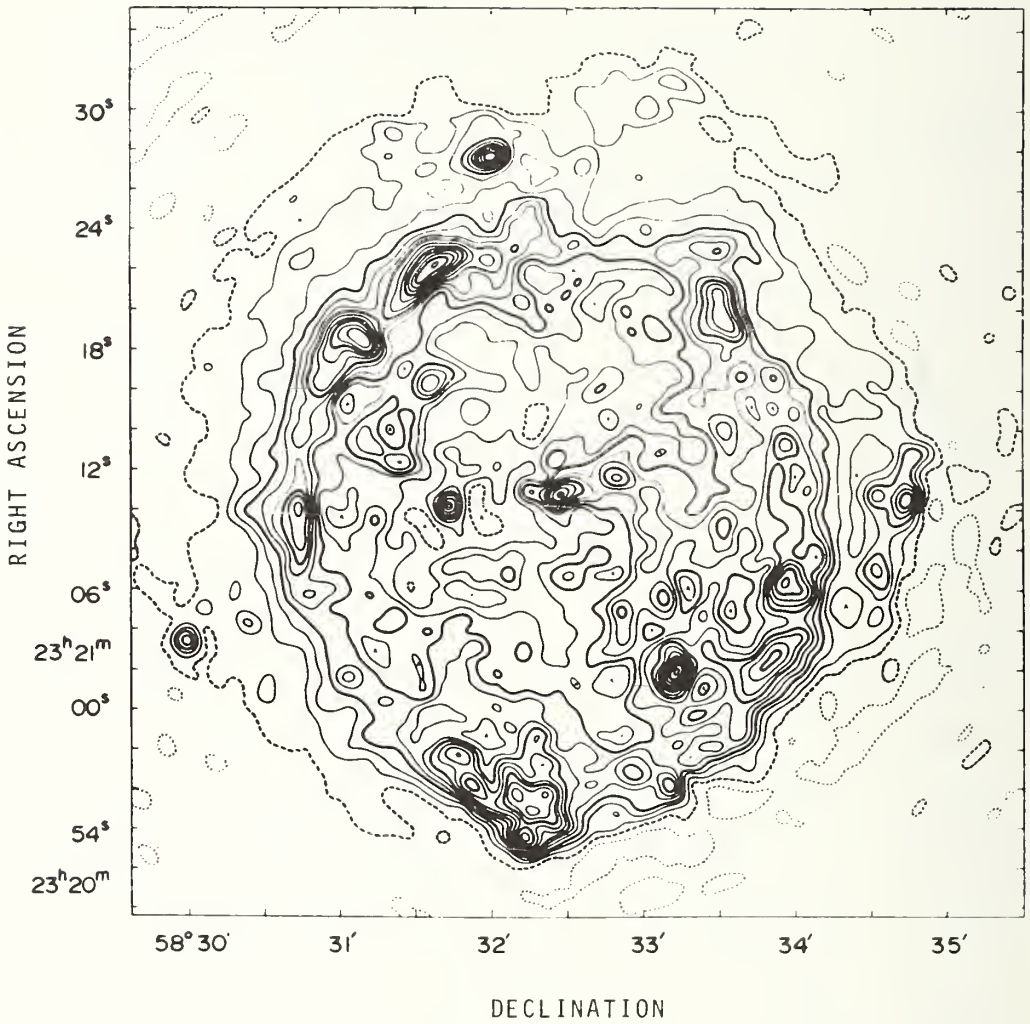

Figure 3. Brightness temperature contour map of Cas A (coordinates for Epoch AD 1950.0, after Rosenberg 1970b)

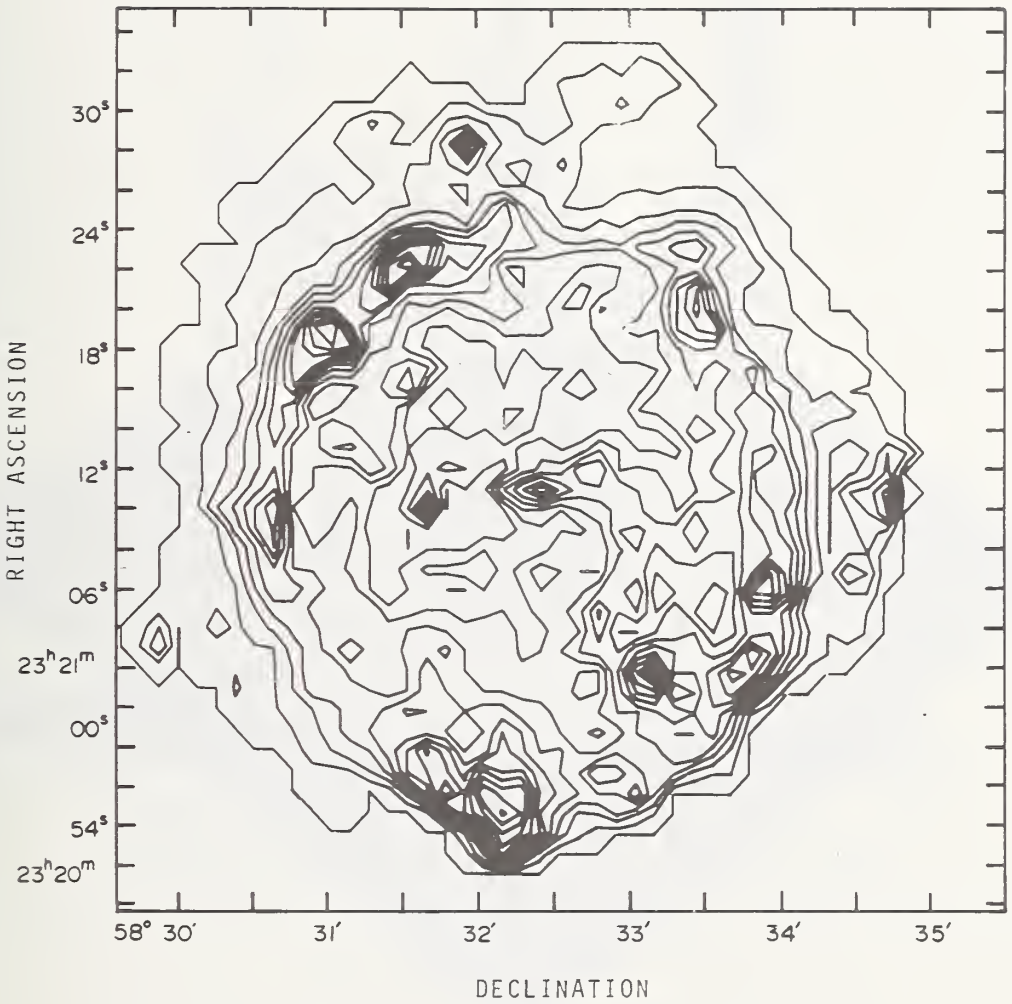

Figure 4. Reconstructed brightness temperature contour map of Cas A

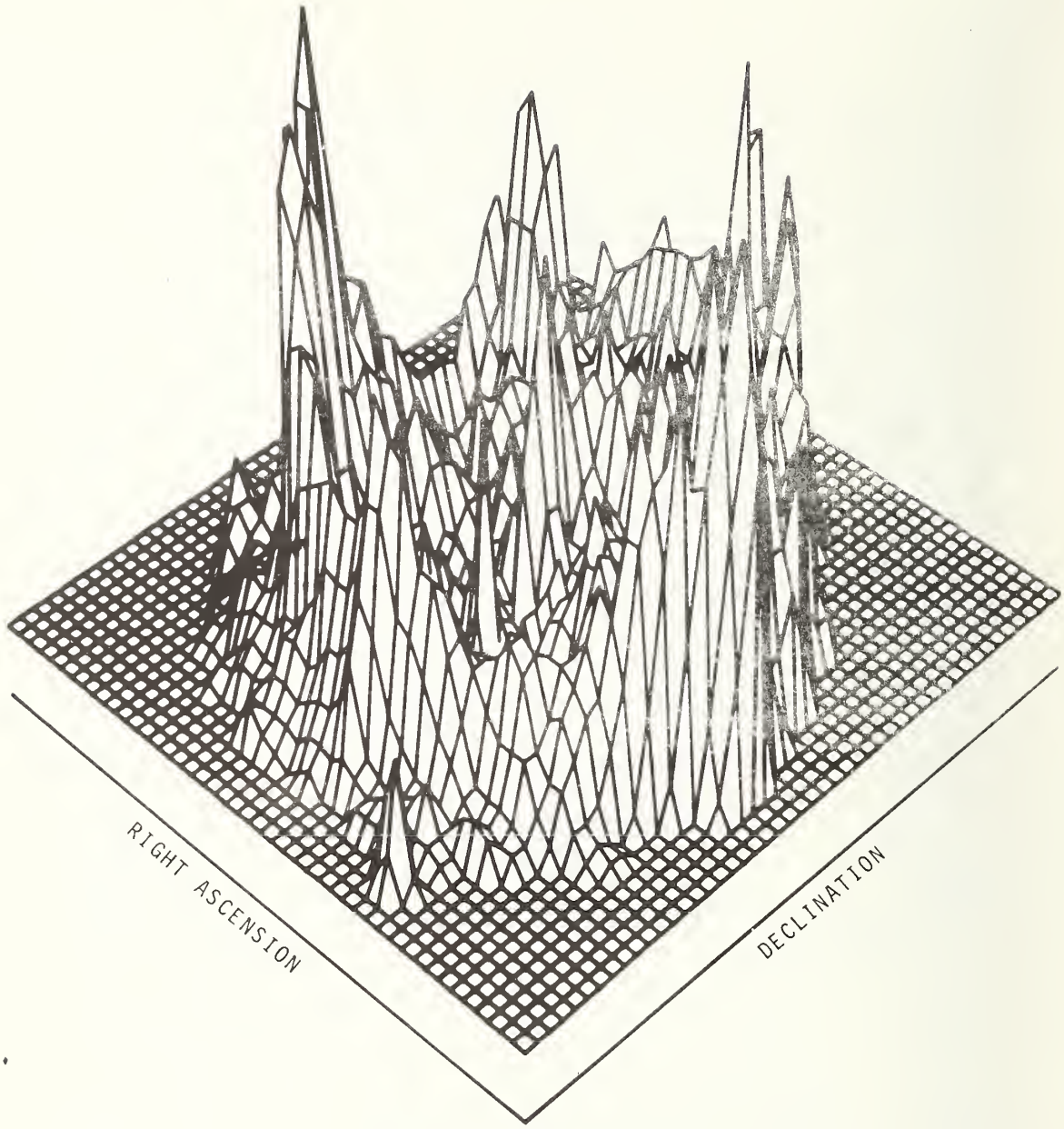

Figure 5. Three-dimensional representation of Cas A brightness temperature

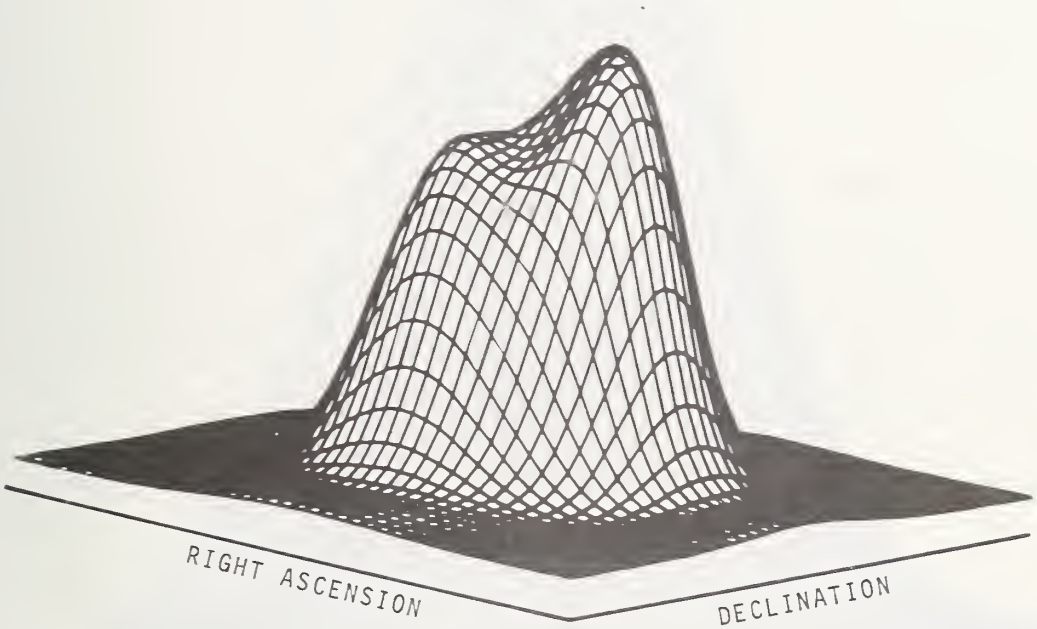

Figure 6. Three dimensional representation of convolution integral of Cas A with 2 minutes antenna half-power beamwidth

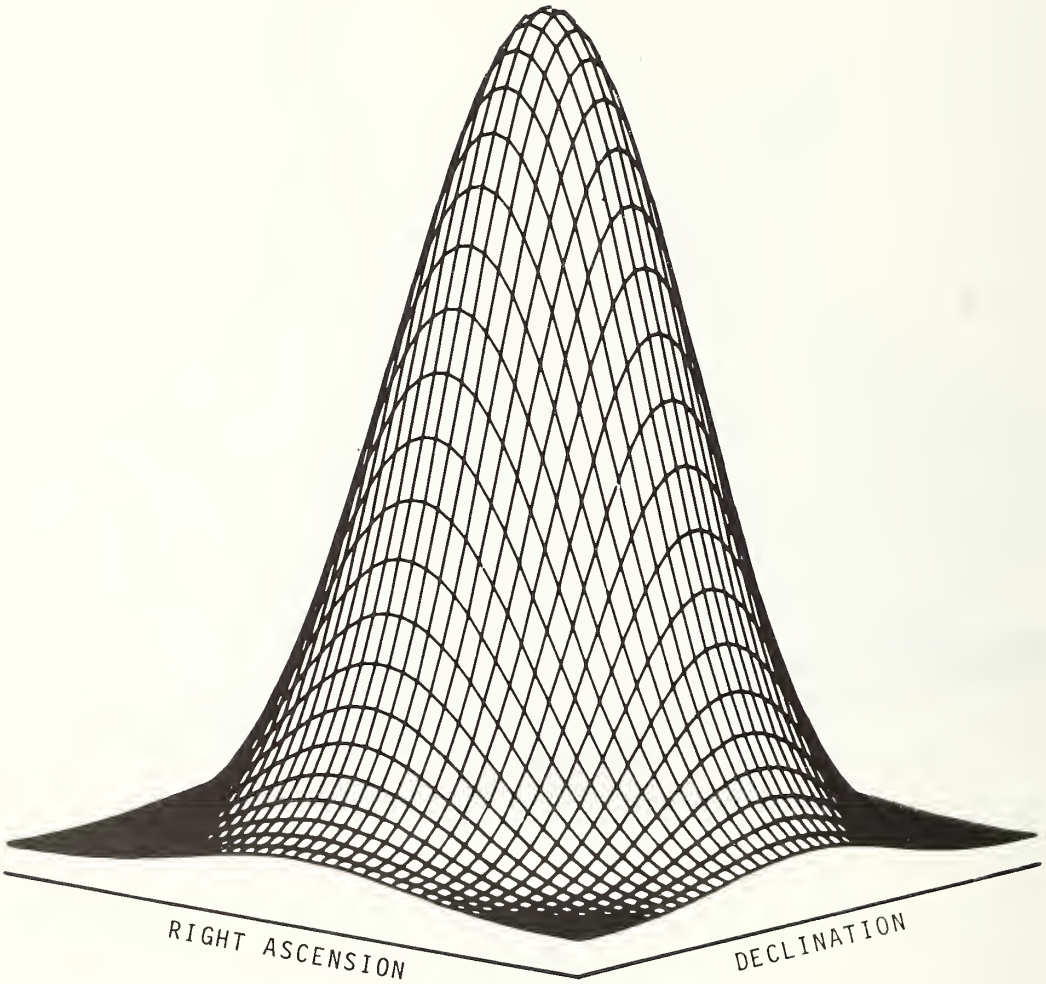

Figure 7. Three dimensional representation of convolution integral of Cas A with 4 minutes antenna half-power beamwidth

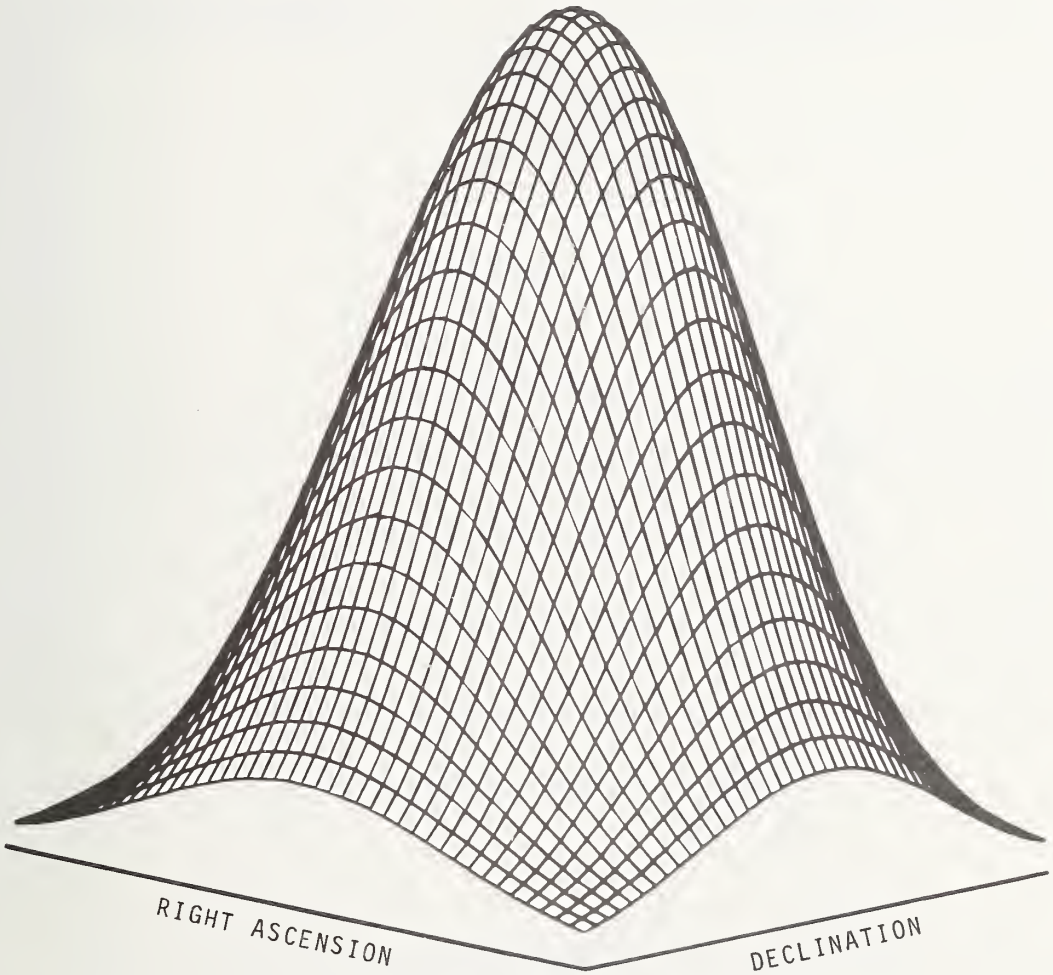

Figure 8. Three dimensional representation of convolution integral of Cas A with 6 minutes antenna half-power beamwidth

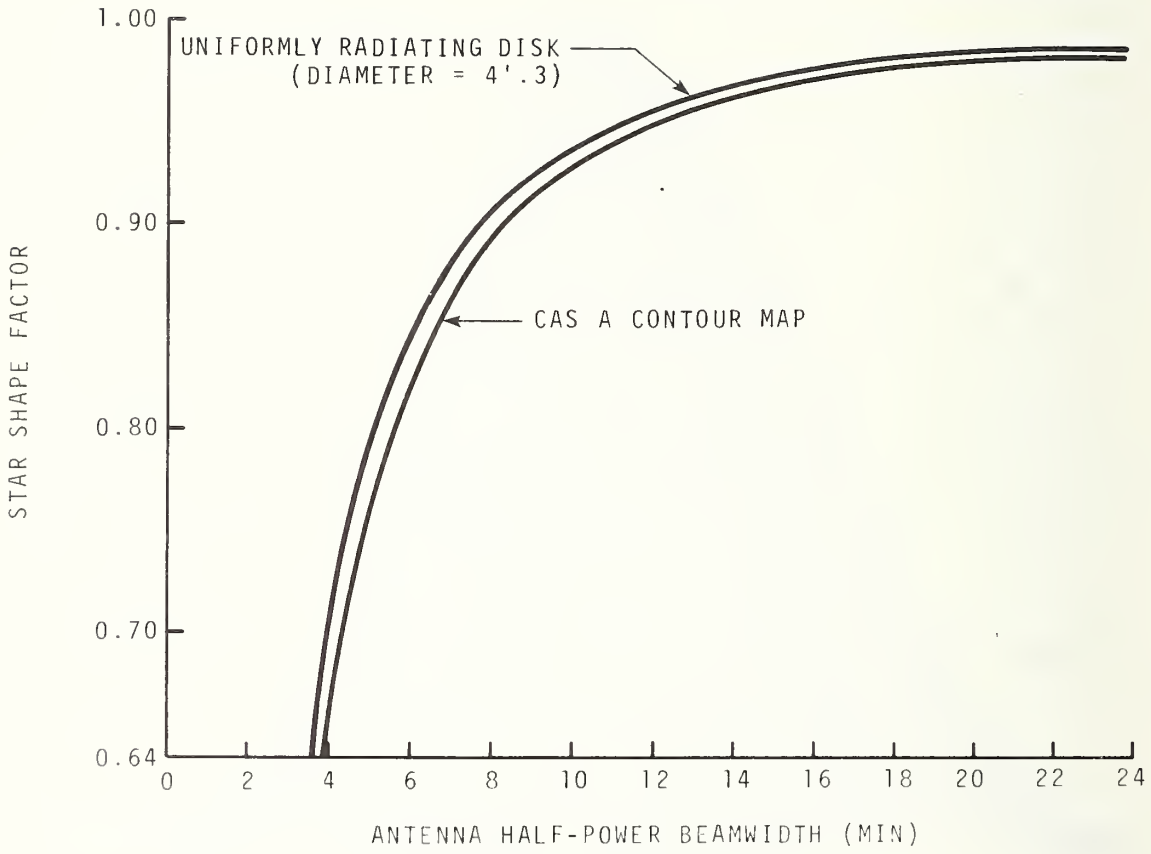

Figure 9. Star shape factor, k_2, versus antenna half-power beamwidth

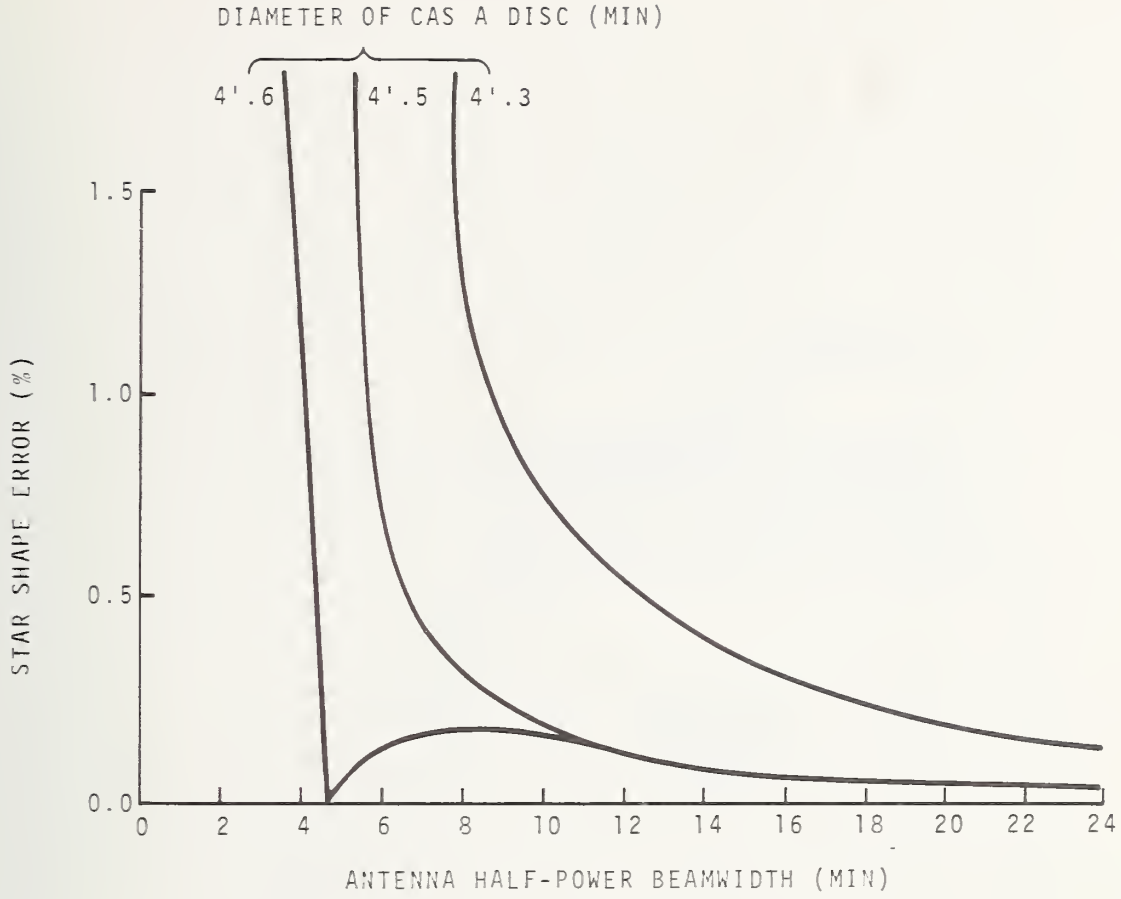

Figure 10. Star shape factor error versus antenna half-power beamwidth

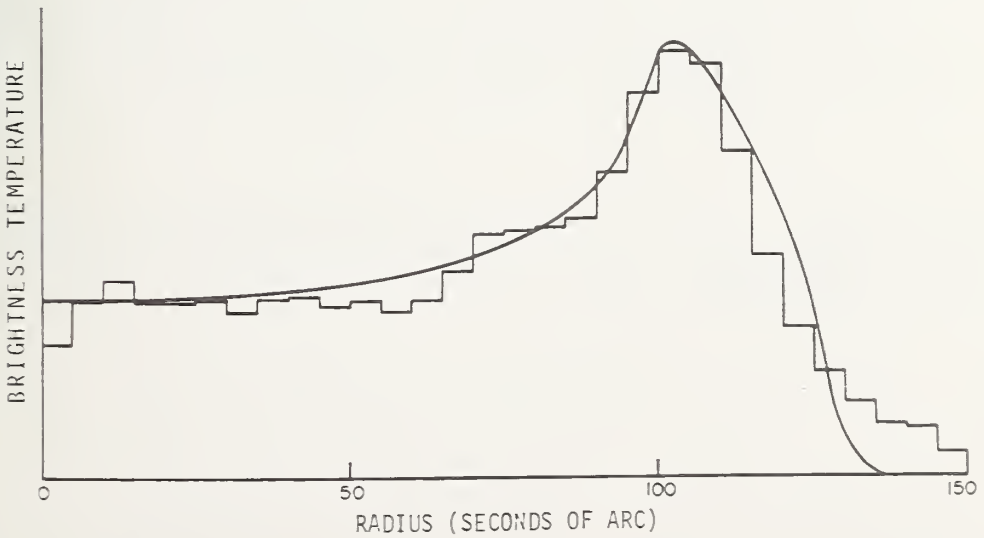

Figure 11. Mean brightness temperature profile from the center of Cas A outward (Epoch AD 1950.0, 5.0 GHz, after Rosenberg 1970b)

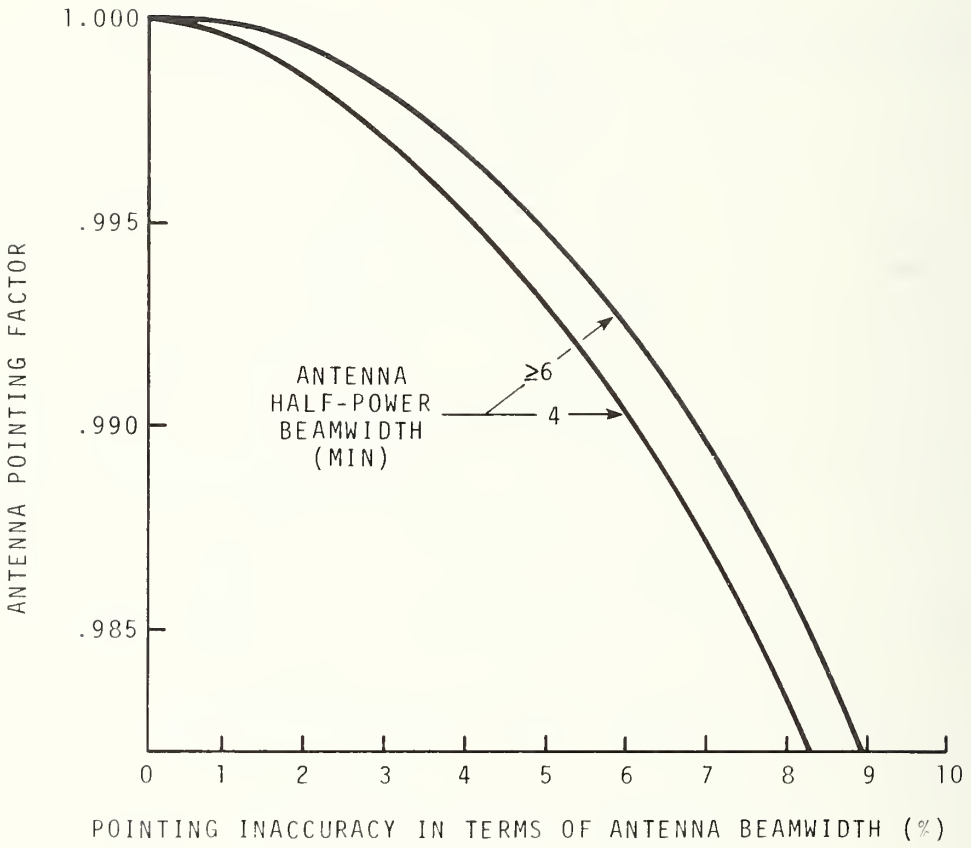

Figure 12. Antenna pointing factor, k_5, versus antenna half-power beamwidth

Figure 13. Antenna pointing factor, k_5, versus a number of drift cuts across Cas A

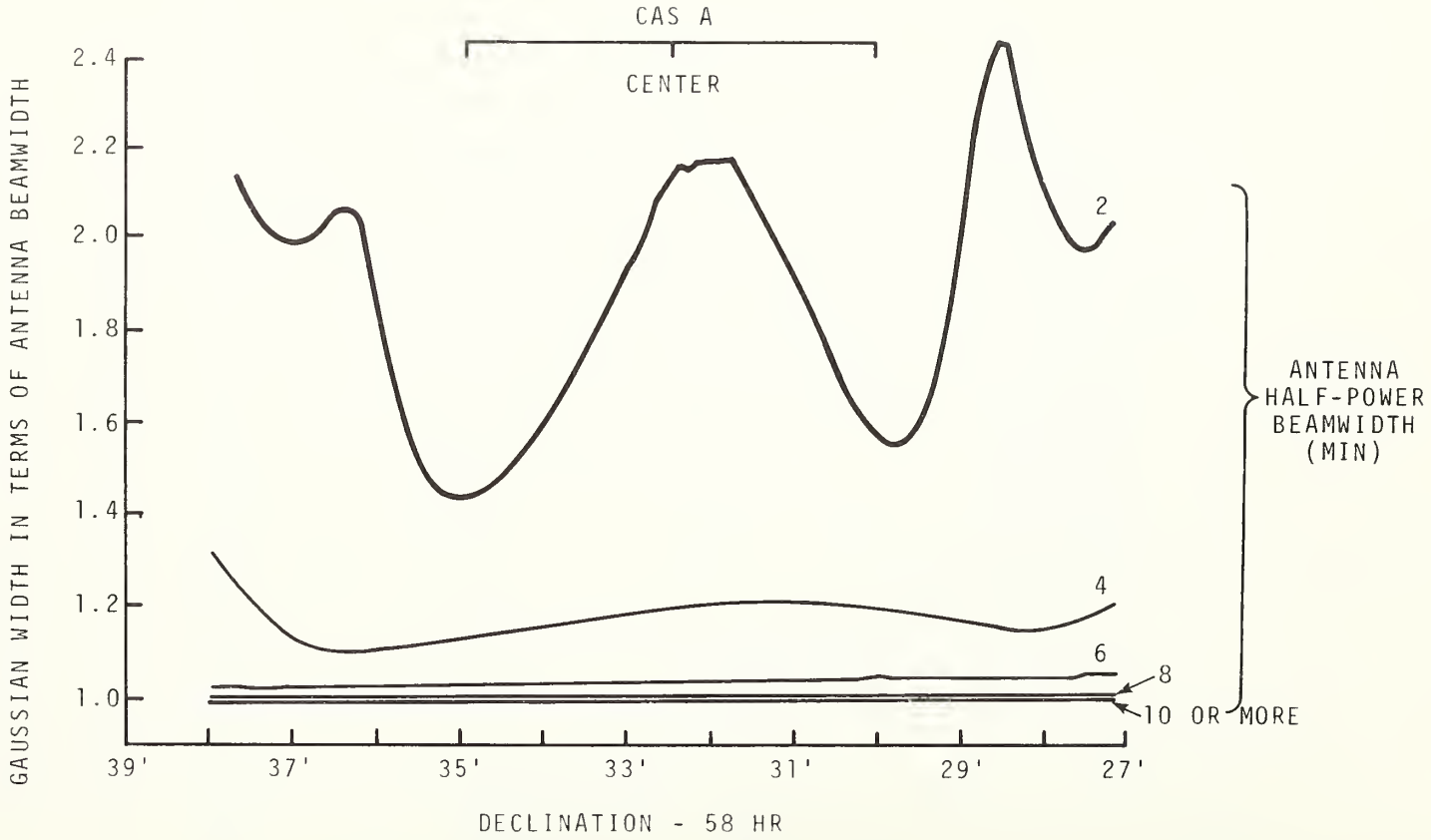

Figure 14. The width of the Gaussian fitting for drift curves versus location of drift cut across Cas A

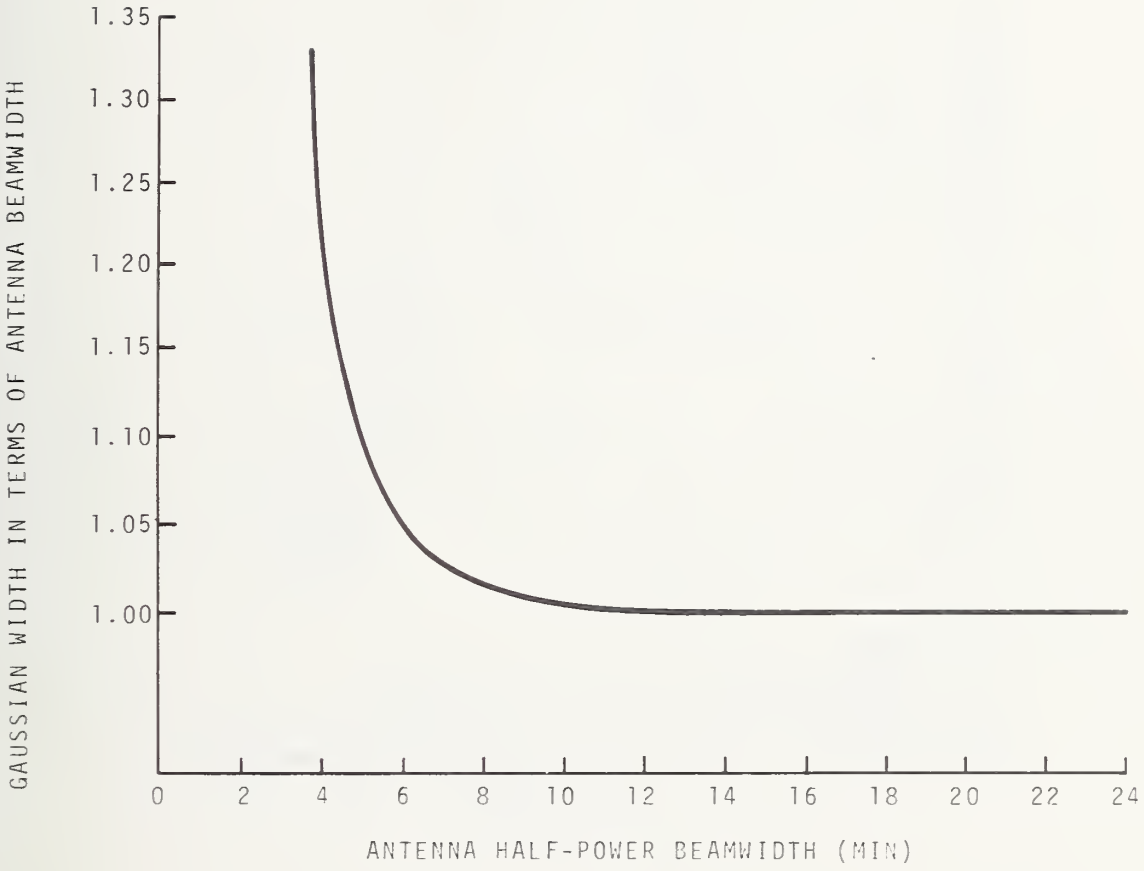

Figure 15. The width of the Gaussian fitting for drift curves versus antenna half-power beamwidth

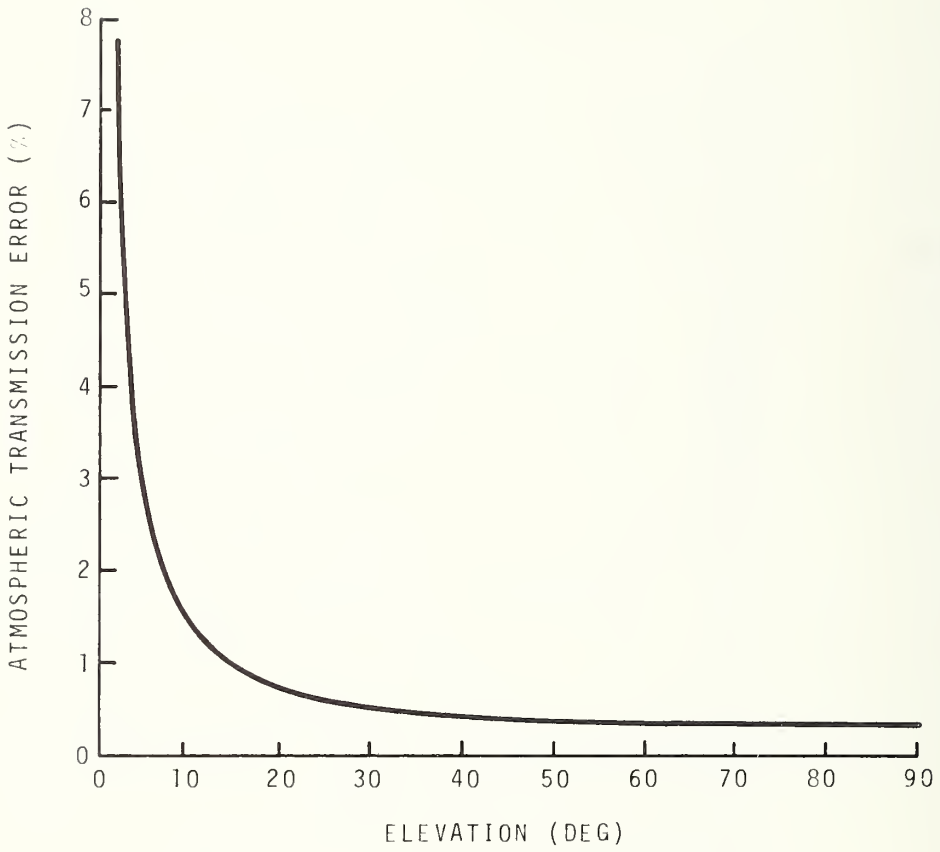

Figure 16. Atmospheric transmission factor error versus elevation angle (after Daywitt 1975)

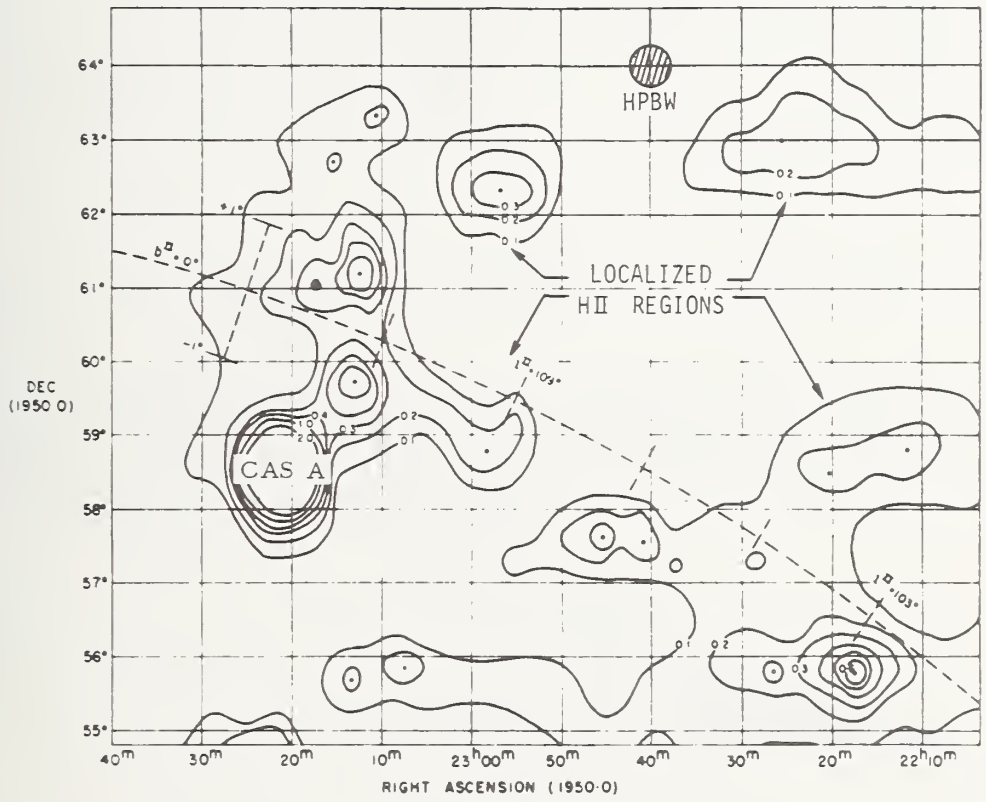

Figure 17. Cosmic radio background around Cas A at 3.2 GHz (after RaghavaRao et al. 1965)

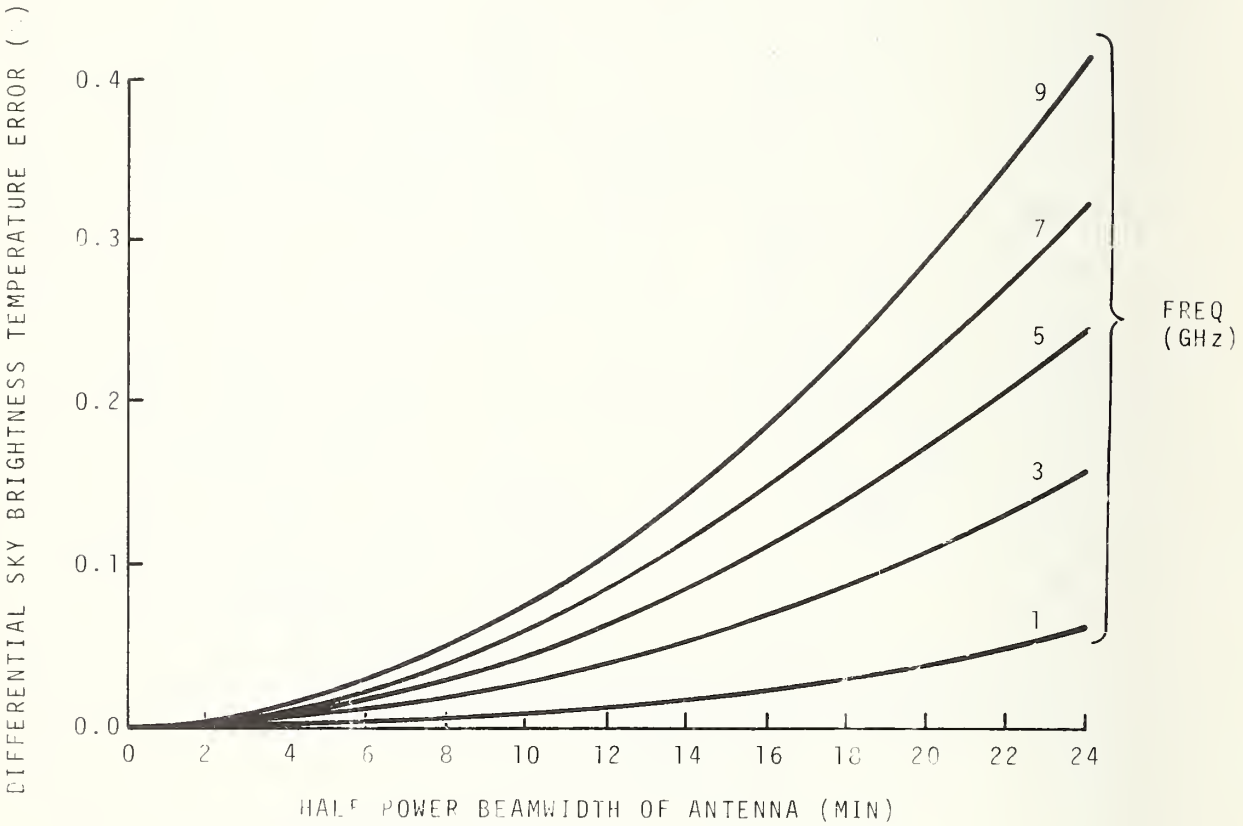

Figure 18. Differential sky brightness temperature factor, k_4, versus half-power beamwidth

NBS-114A (REV. 7-73)

U.S. DEPT. OF COMM. BIBLIOGRAPHIC DATA SHEET	1. PUBLICATION OR REPORT NO. NBSIR 75-822	2. Gov't Accession No.	3. Recipient's Accession No.

4. TITLE AND SUBTITLE

Study of Errors in Absolute Flux Density Measurements of Cassiopeia A

5. Publication Date: October 1975

6. Performing Organization Code: 276.06

7. AUTHOR(S): Motohisa Kanda

8. Performing Organ. Report No.: NBSIR 75-822

9. PERFORMING ORGANIZATION NAME AND ADDRESS

NATIONAL BUREAU OF STANDARDS, Boulder Labs
DEPARTMENT OF COMMERCE
WASHINGTON, D.C. 20234

10. Project/Task/Work Unit No.: 2766482

11. Contract/Grant No.

12. Sponsoring Organization Name and Complete Address (Street, City, State, ZIP)

U. S. Army Communications Command
Fort Huachuca, Arizona 85613

13. Type of Report & Period Covered

14. Sponsoring Agency Code

15. SUPPLEMENTARY NOTES

16. ABSTRACT (A 200-word or less factual summary of most significant information. If document includes a significant bibliography or literature survey, mention it here.)

An error analysis for absolute flux density measurements of Cassiopeia A is discussed. The lower-bound quadrature-accumulation error for state-of-the-art measurements of the absolute flux density of Cas A around 7 GHz is estimated to be 1.71% for 3σ limits. The corresponding practicable error for the careful but not state-of-the-art measurement is estimated to be 4.46% for 3σ limits.

17. KEY WORDS (six to twelve entries; alphabetical order; capitalize only the first letter of the first key word unless a proper name; separated by semicolons)

Accuracy; antenna; calibration; Cassiopeia A; error analysis; flux density; G/T (system gain/system noise temperature); ground station; radio star.

18. AVAILABILITY

[X] Unlimited

[ ] For Official Distribution. Do Not Release to NTIS

[ ] Order From Sup. of Doc., U.S. Government Printing Office Washington, D.C. 20402, SD Cat. No. C13

[X] Order From National Technical Information Service (NTIS) Springfield, Virginia 22151

19. SECURITY CLASS (THIS REPORT)	21. NO. OF PAGES
UNCLASSIFIED	34
20. SECURITY CLASS (THIS PAGE)	22. Price
UNCLASSIFIED	$ 3.75

USCOMM-DC 29042-P74

USCOMM · ERL